Original Article

Bulletin of Pure and Applied Sciences.
Vol.37 C (Chemistry), No.1, 2018: P.27-35
Print version ISSN 0970 4620
Online version ISSN 2320 320X
DOI 10.5958/2320-320X.2018.00005.5

Optical and dielectric investigations of nano crystalline scheelite $A_{0.5}B_{0.5}MoO_4$ (A=B=Ba, Sr and Ca)

S. Vidya[1]*, J.K. Thomas[2]

Author Affiliations
[1]Department of Physics, Sree Narayana College, Kollam, India - 691001
[2]Electronic Materials Research Laboratory, Department of Physics, Mar Ivanios College, Thiruvananthapuram, Kerala, India-695 015

Corresponding Author
***S. Vidya,** Department of Physics, Sree Narayana College, Kollam, India – 691001

E-mail: vidyaasnair@gmail.com

Received on 17th January 2018
Accepted on 31st January 2018

Abstract

The synthesis of nanocrystalline $A_{0.5}B_{0.5}MoO_4$ by an auto-igniting combustion technique is reported. The structural characterization done by X–ray diffraction, Fourier transform Raman spectroscopy and infrared spectroscopy reveals that the as-prepared powder itself is phase pure with tetragonal structure. The particle size determined from Transmission electron microscopy are in the range 23–25 nm. The optical band gap determined show that the compounds are wide bandgap semiconductors. The photoluminescence spectrum of $A_{0.5}B_{0.5}MoO_4$ shows green emission, associated with the perfect order and crystallinity of the sample. All the samples are sintered at a temperature less than 875°C. The dielectric constant and loss factor of the samples are measured at radiofrequency range and its variation with temperature is also studied. The effect of change in composition of A^{2+} site of scheelite AMO_4 compounds comparative are also presented. The experimental results show that nano $A_{0.5}B_{0.5}MoO_4$ is an excellent luminescent material and also a promising 'Low temperature Co–fired Ceramic. Also it is inferred that we can fine tune both optical and dielectric properties to desired values according to our requirements by adjusting the cationic stoichiometric ratio in $[AO_8]$ octahedron.

Keywords: nanocrystalline, scheelite, AMO_4 compounds, FT Raman

1. INTRODUCTION

The quest for new and novel materials with excellent properties is increasing day by day due to the rapid technological development and processing techniques all over the world. Materials in the form of crystals, films, micron to nano sized powders and composites have caught much attention of the researchers. Among them, nanomaterials stand prominent due to their exceptional properties which are completely different from their other forms.

Scheelite compounds characterized by tetragonal structure with general formula AMO_4 are extensively studied due to their remarkable optical and electrical properties and wide range of applications including solid-state lasers, optic fibre, stimulated Raman scatters, low-temperature radiation detectors, scintillators and microwave applications [1–5]. The unique properties of these materials can be tailored by trying different stoichiometric ratios or combinations of these compounds such as $A_xB_{1-x}MO_4$, $AMo_xW_{1-x}O_4$ etc. Only a few reports have appeared in literatures on such combinations of scheelite group materials and their vast potential has not yet been exploited. The structural properties and photoluminescence behaviour in the $Ca_xSr_{1-x}WO_4$ system at room temperature was investigated by Porto et al [6] and that of $Ba_{0.5}Sr_{0.5}MoO_4$ by Wei et al [7]. Zhuravlev et al [8] has studied the stability of solid solutions in scheelite type molybdates and tungstates. $Sr_{1-x}Ca_xWO_4$ solid–solution films were prepared by Cho and Yoshimura [9]. Red–luminescence phosphors $Ca_{0.5}Sr_{0.5}MoO_4:Eu^{3+}$ for white LED have been reported by Shi et al [10]. The gas sensing property of $Ba_{0.5}Sr_{0.5}MoO_4$ thick film [11] and the enhancements of magneto resistance in $La_{0.7}Ca_{0.15}Sr_{0.15}Mn_{1-x}Mo_xO_3$ compound have also been investigated [12]. The different synthesis techniques used in these studies are soft chemical method [6], molten salt method, citrate method [8], sol–gel method [10] and solid state reaction [12, 13]. The preparation of $Ba_{1-x}Sr_xWO_4$ and $Ba_{1-x}Ca_xWO_4$ films by mechanically assisted solution reaction by Rangappa et al [14] at room temperature has also been reported.

Among the reported works much attention is devoted to the tuning of luminescence properties of the scheelite compounds while studies on its dielectric properties, sintering behaviour, band gap studies remain restricted. In view of this fact in mind we had made an attempt to study the structural, optical, sintering and dielectric behaviour of $Ba_{0.5}Sr_{0.5}MoO_4$, $Sr_{0.5}Ca_{0.5}MoO_4$ and $Ba_{0.5}Ca_{0.5}MoO_4$ of nanopowder synthesized through a modified combustion technique, for the first time. Brief comparisons between the parent compounds $AMoO_4$ and the compositions were also presented in the chapter and its suitability for various applications have also been discussed.

2. EXPERIMENTAL

Similar procedure was adopted for the preparation of the compositions $A_{0.5}B_{0.5}MO_4$ (A=B=Ba, Sr, and Ca) through modified combustion technique. The only distinction is in the stoichiometric amount of initial reagents to be taken.

As a typical instance, the preparation of $Ba_{0.5}Sr_{0.5}MoO_4$ nanopowder through the modified combustion process was detailed. For the preparation of $Ba_{0.5}Sr_{0.5}MoO_4$, aqueous solutions containing Ba, Sr and Mo ions were prepared by dissolving stoichiometric amounts of $Ba(NO_3)_2$, $Sr(NO_3)_2$ and ammonium molybdate in double distilled water. Citric acid was then added to the solution as complexing agent. The amount of citric acid to be added was calculated based on the total valence of the oxidizing and the reducing agents for maximum release of energy during combustion. Oxidant to fuel ratio of the system was adjusted by adding concentrated nitric acid and ammonium hydroxide solution and the ratio was kept at unity. The precursor solution of pH ~7.0 was stirred well for uniform mixing and a clear solution with no precipitate or sedimentation was obtained. The solution was then heated using a hot plate at ~250 °C in a ventilated fume hood. The solution boils on heating and undergoes dehydration accompanied by foam. On persistent heating the foam gets autoignited giving a voluminous fluffy powder of nano $Ba_{0.5}Sr_{0.5}MoO_4$. Thus obtained nano powder itself is used for further characterisation. A similar pattern was followed in case of $Sr_{0.5}Ca_{0.5}MoO_4$ and $Ba_{0.5}Ca_{0.5}MoO_4$.

Structure of the as-prepared powder was examined by powder X-ray diffraction (XRD) technique using a Bruker D–8 X-ray Diffractometer with Nickel filtered Cu Kα radiation. Particulate properties of the combustion product were examined using transmission electron microscopy (TEM, Model-Hitachi H-600 Japan) operating at 200 kV. The Infrared (IR) spectra of the samples were recorded in the range 400–4000 cm^{-1} on a Thermo-Nicolet Avatar 370 Fourier Transform Infrared (FTIR) Spectrometer using KBr pellet method. The Fourier transform–Raman spectra of the samples were carried out at room temperature in the wave number range 50–1200 cm-1 using Bruker RFS/100S

Spectrometer. The photoluminescence (PL) spectra of the samples were measured using Flurolog@-3 Spectroflurometer. For low frequency dielectric studies the pellets were made in the form of a disc capacitor with the specimen as the dielectric medium. Both the flat surfaces of the sintered pellet were polished and then electroded by applying silver paste. The capacitance of the sample was measured using an LCR meter (Hioki–3532–50 LCR HiTester) in the frequency range 100 Hz–5 MHz at different temperature from 30–250 °C.

3. RESULTS AND DISCUSSIONS

3.1. STRUCTURAL ANALYSIS

3.1.1. XRD Analysis

The XRD pattern of as-prepared $Ba_{0.5}Sr_{0.5}MoO_4$, $Sr_{0.5}Ca_{0.5}MoO_4$ and $Ba_{0.5}Ca_{0.5}MoO_4$ nanopowder is shown in the figure 1. All the peaks are indexed for a perfect tetragonal structure based on the spectral data in the JCPDS file 30-0157 for $Ba_{0.5}Sr_{0.5}MoO_4$ and file 30-1287 for $Sr_{0.5}Ca_{0.5}MoO_4$. The XRD pattern of $Ba_{0.5}Ca_{0.5}MoO_4$ is found to be iso-structural with the other two compounds of similar composition. Thus $Ba_{0.5}Ca_{0.5}MoO_4$ also possesses tetragonal structure and the XRD pattern is indexed on the basis of JCPDS files reported for $Ba_{0.5}Sr_{0.5}MoO_4$ and $Sr_{0.5}Ca_{0.5}MoO_4$.

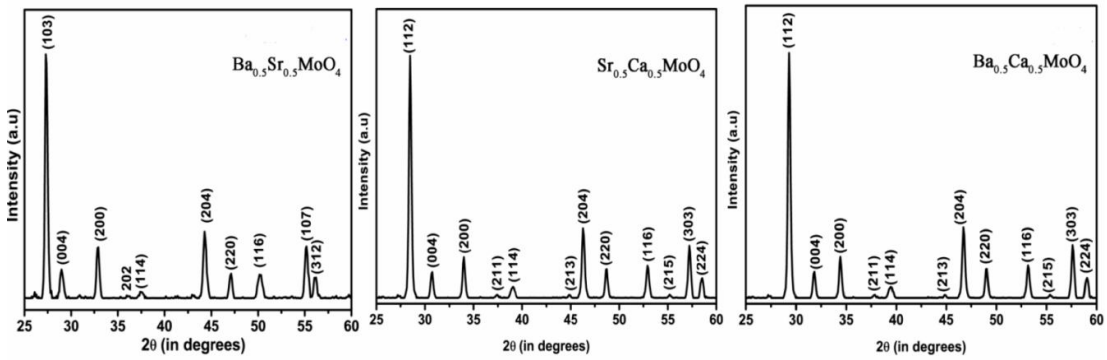

Fig. 1: XRD pattern of as-prepared nano $A_{0.5}B_{0.5}MoO_4$ (A=B=Ba, Sr, Ca)

Table 1: Calculated lattice parameters, unit cell volume and crystallite size estimated by the Scherer formulae

Compounds	Crystal Structure	Experimental lattice parameters (Å)	Unit cell Volume ($Å^3$)	Crystallite size (nm)
$Ba_{0.5}Sr_{0.5}MoO_4$	Tetragonal	a=b=5.490, c=12.495	376.006	23
$Sr_{0.5}Ca_{0.5}MoO_4$	Tetragonal	a=b=5.310, c=11.759	331.557	22
$Ba_{0.5}Ca_{0.5}MoO_4$	Tetragonal	a=b=5.482, c=12.488	375.293	24

No additional peak representing impurities or secondary phase or un-reacted multi could be observed in the XRD patterns. This suggests that all the compounds are single phase with scheelite structure. Thus the XRD patterns confirm that the modification of cation ratio in the A^{2+} site of AMO_4, did not lead to structural transformation. This may be due to the fact that all the substituted elements (Ba, Sr, Ca) have comparable ionic radii as they belong to same group of the periodic table. So they adhere well into the lattice structure without structure distortion. Phase formation was also complete during the combustion process itself, without any calcination step. Thus the modified combustion method for the synthesis of nanopowder offers an economic and time saving technique.

3.1.2. Vibrational Spectroscopic Studies

In order to study the vibrational spectra and conduct a detailed structural investigation, Raman and FTIR spectra of $A_{0.5}B_{0.5}MoO_4$ is recorded which are given in figure 2, and 3, respectively.

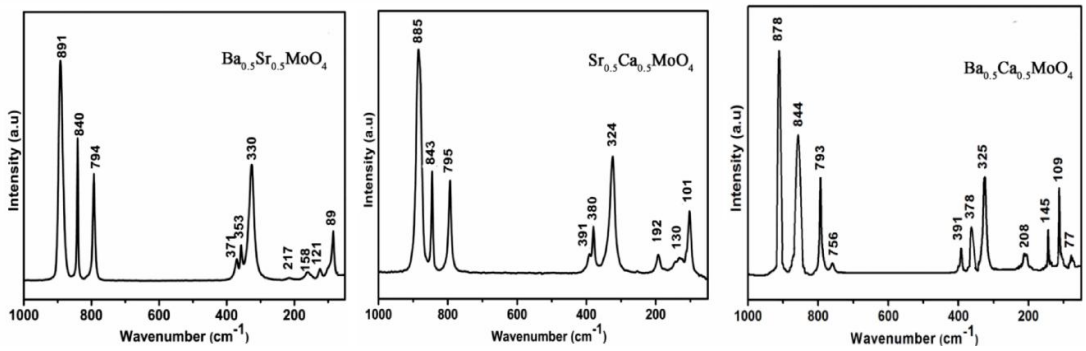

Fig. 2: Raman spectra of as-prepared nano $A_{0.5}B_{0.5}MoO_4$ (A=B=Ba, Sr, Ca)

On comparison with the vibrational spectra reported for the compounds $BaMoO_4$, $SrMoO_4$, $CaMoO_4$, $BaWO_4$, $SrWO_4$ and $CaWO_4$, the sample $A_{0.5}B_{0.5}MO_4$ also seem to exhibit a similar spectral pattern with respective shifts in the wave number positions [15–19].

The internal modes include the vibrational and rotational modes of the tetrahedron and are observed in the region 900−180 cm^{-1} whereas the external group consists of lattice phonon modes corresponding to the motion of Ba^{2+} /Sr^{2+} cations and the rigid molecular units and are attributed to peaks in the region 160−78 cm^{-1}.

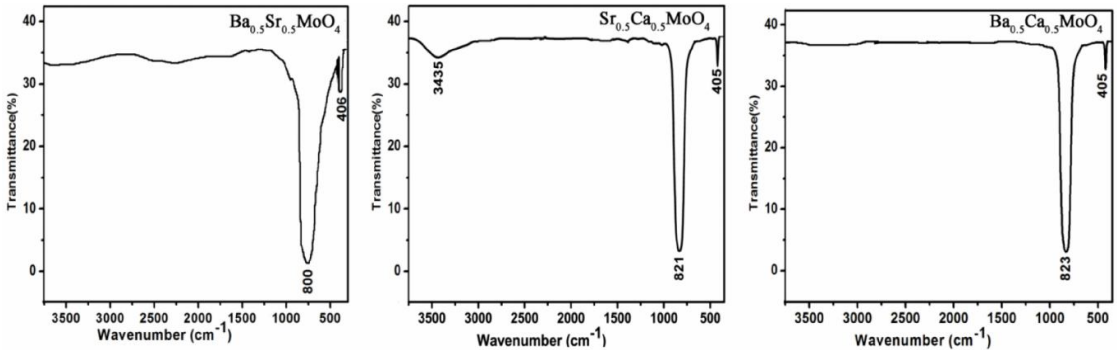

Fig. 3: FTIR spectra of as-prepared nano $A_{0.5}B_{0.5}MoO_4$ (A=B=Ba, Sr, Ca)

The most intense band of Raman spectra observed above 850 cm^{-1} in all the spectra are attributed to the A_g mode of vibrations. The B_g modes are assigned to peaks in the wave number range 845–830 cm^{-1}.The next highest bands of Raman spectra responds to internal mode of vibration, Eg..The modes involving the free rotation in the limiting case of the uncoupled MoO_4 ions in $Ba_{0.5}Sr_{0.5}MoO_4$, $Sr_{0.5}Ca_{0.5}MoO_4$, $Ba_{0.5}Ca_{0.5}MoO_4$ are observed above 200 cm^{-1} which has the E_g symmetry. This vibration mode shows highest wave number shift on comparing with AMO4 compounds where this mode is assigned to peaks around 180 cm^{-1}. The external modes $2B_g$ and $2E_g$ are assigned to the lowest frequency bands.

The IR spectrum shows a very strong absorption a band in which higher wavenumber is due to Metal–Oxygen (M–O) stretching vibration mode and the latter due to the weak Metal– Oxygen (M–O) bending vibration. These correspond to the IR active ν_3A_u and ν_4A_u modes of vibrations.

The splitting up of non-degenerate peaks, superposition of certain peaks into a broad peaks, small shift in the vibration mode frequencies, inactivity of certain active peaks in the Raman spectra of the compounds points to lowering of symmetry of the crystal structure. Thus all these compositions possess certain degree of shot range structural disorder. However there is no evidence for secondary phase or any other impurities. A trace of MoO_3 unit which was noticed in the Raman spectra of

$SrMoO_4$ was absent in this case. So the distortion is only short range. The vibrational analysis confirms the XRD result that $A_{0.5}B_{0.5}MO_4$ own tetragonal structure.

3.2. TEM analysis

The TEM studies on the morphology of the as-prepared nanopowder obtained by the combustion route are shown in the figure 4. The micrograph showed that the particles are of submicron size in the range of 20–25 nm. The nano particles of all the compounds possess nearly spherical morphology and the absence of agglomeration of the particles indicates the good nanocrystalline nature of the sample. The majority particle size obtained from the TEM are 23nm, 22nm and 25nm for A0.5B0.5MO4 (A=B=Ba, Sr, Ca) respectively.

SAED patterns are composed of a number of bright spots arranged in concentric rings. The ring nature of the electron diffraction pattern is indicative of the polycrystalline nature of the crystallites, but the spotty nature is due to the fact that the fine crystallites having related orientations are agglomerated together resulting in a limited set of orientations.

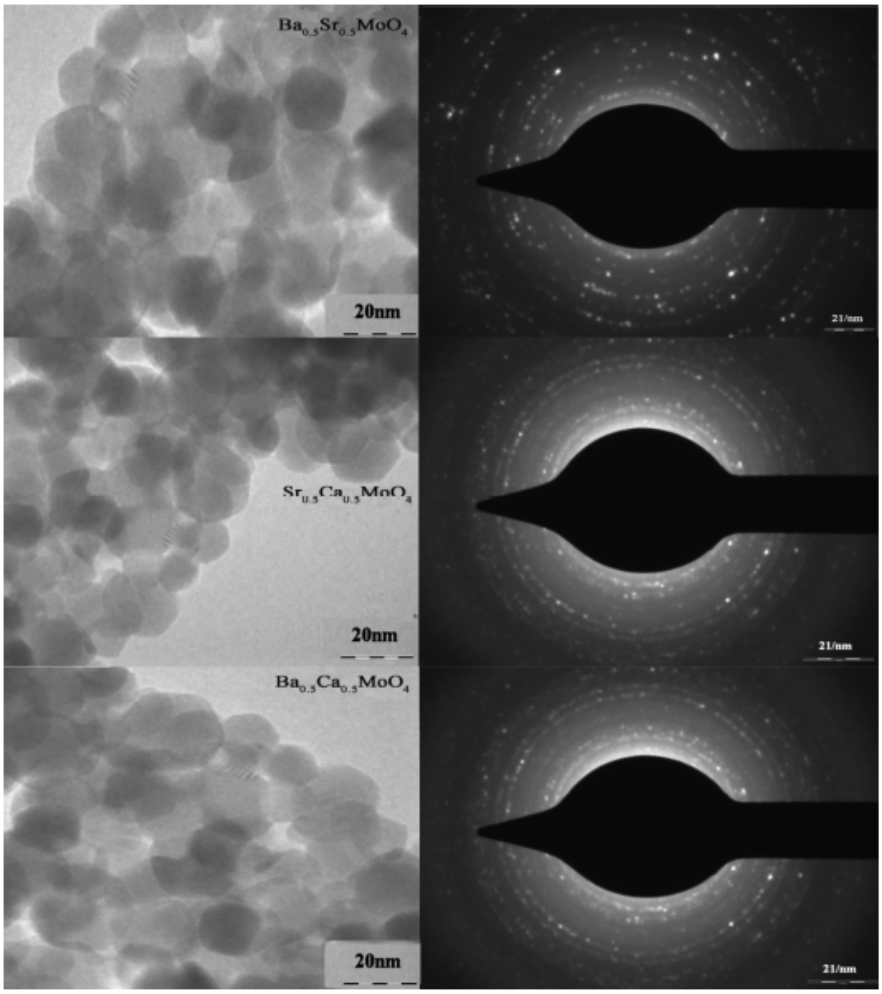

Fig. 4: TEM image of as-prepared nano $A_{0.5}B_{0.5}MoO_4$ (A=B=Ba, Sr, Ca)

3.3. Optical properties

3.3.1. Photoluminescent Studies

The PL emission spectrum of $A_{0.5}B_{0.5}MoO_4$ nano powder is shown in the figure 6. The sample shows intense green emission. The reason for the PL emission of scheelite structure is explained in literatures in many ways viz. due to structural disorder, morphology, charge–transfer transitions into

the $[MoO_4]^{2-}$ complex, the existence of MoO_3 and distorted MoO_4 complex clusters, particle sizes, crystalline degree, morphology, and surface defects [24–26].

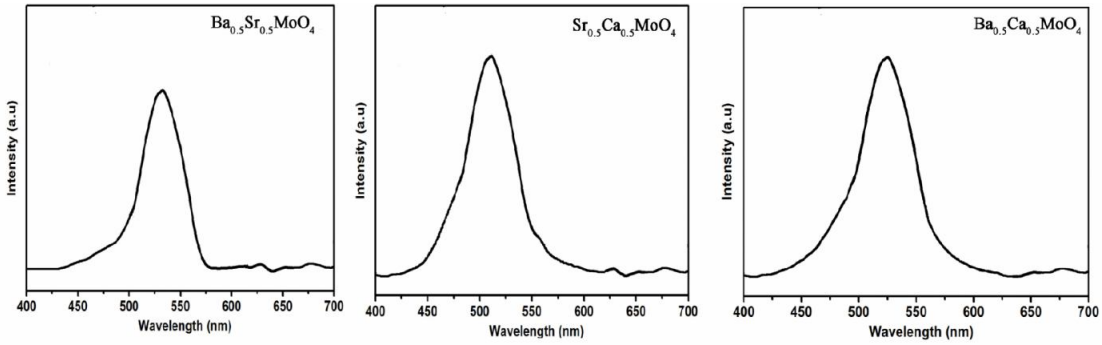

Fig. 5: PL spectra of $A_{0.5}B_{0.5}MoO_4$ (A=B=Ba, Sr, Ca)

For our sample, as there is no long range structural disorder, the main reason for the green emission in the PL emission spectrum can be the charge–transfer transitions within the $[MoO_4]^{2-}$ complex, in the ordered system. Wei et al reported a blue emission for $Ba_{0.5}Sr_{0.5}MoO_4$ and ascribed it to the $^1T_2 \rightarrow {}^1T_1$ electronic transitions into the $[MoO_4]$ tetrahedron groups [7]. A striking green luminescence was observed by varying the ratio of Ca and Sr in $Sr_{1-x}Ca_xMoO_4:Tb^{3+}$ by Wang et al [27]. The PL emission of $BaMoO_4$ $SrMoO_4$ and $CaMoO_4$ prepared through the same combustion method also showed an intense green emission along with a weak red emission which is because of the presence of MoO_3–MoO_4 clusters and on annealing, the red emission peak vanished [20,21]. Thus the observed green emission is associated with the perfect order and crystallinity of the sample.

Accordingly we can also make out that luminescence behaviour primly depends on $[MoO_4]^{2-}$ in molybdates scheelite class of compounds. The change of stochiometry in A^{2+} of AMO_4 could persuade a small wavelength shift. Hence when the composition is altered systematically as A_1 and $B_{(1-x)}$, we can obtain different compositions which yield blue emission as well as green emission. Thus we can fine tune the PL emissions which have much advantage in laser applications.

3.4. SINTERING

The sintering behaviour of the nanocrystals of $A_{0.5}B_{0.5}MO_4$ powder synthesized through the present combustion route was studied.

Table 2: Sintering temperature, soaking time and relative density of sintered AMO_4 and $A_{0.5}B_{0.5}MO_4$ (A=B=Ba, Sr, Ca and M=Mo, W)

Compounds	Sintering temperature (°C)	Soaking time (h)	Relative Density achieved (%)
$BaMoO_4$	750	3	95
$SrMoO_4$	850	2	96
$CaMoO_4$	775	3	96
$Ba_{0.5}Sr_{0.5}MoO_4$	820	3	96
$Sr_{0.5}Ca_{0.5}MoO_4$	875	3	96
$Ba_{0.5}Ca_{0.5}MoO_4$	800	3	96

A highly sintered specimen was obtained on sintering the compacted nanopowder for all the samples in the temperature range 815-875 °C. The change in composition has influenced the sintering temperatures of the compounds. The sintering temperatures with respective soaking time, density achieved by the compounds along with the same details of AMO_4 compounds prepared by the same method are also depicted in the Table 2.

The change in composition had resulted in an increase of sintering temperature. The maximum density that can be achieved is 96% whereas it is 98% in the case of $SrMoO_4$.The soaking time required for all the compounds are 3 hours. It is to be noted that as all the samples are sintered at a temperatures below 900 °C. Hence these samples are ideal candidates for LTCC applications.

3.5. Dielectric Properties

The dielectric properties of a material determine its functionality. The dielectric behaviour of the sintered samples of $A_{0.5}B_{0.5}MO_4$ nanocrystals are studied in the frequency range 100 Hz to 5MHz. The variation of dielectric constant (ε_r) and the loss factor (tanδ) with frequency are shown in the figure 8.

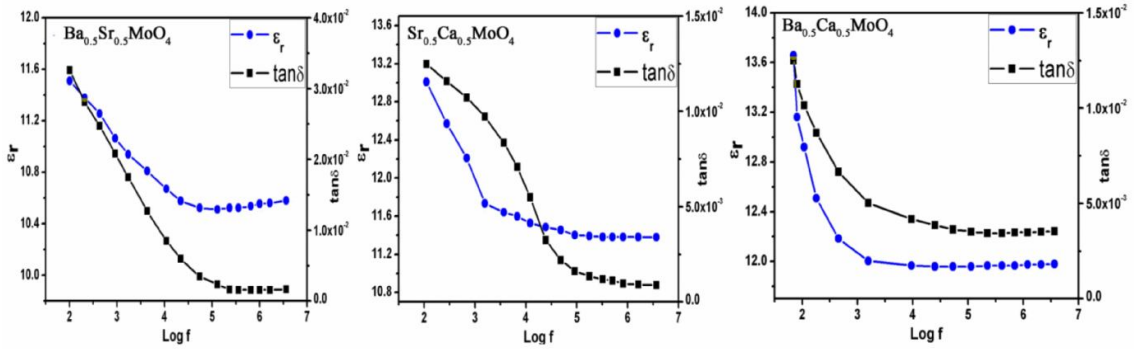

Fig. 8: Variation of ε_r and $\tan_\delta$ with frequency of sintered $A_{0.5}B_{0.5}MoO_4$ (A=B=Ba, Sr, Ca) pellets

The dielectric constant and the loss factor of the samples also show significant change. It can be clearly noted that loss factor decreases as frequency increases while the dielectric constant remains almost unaltered in the high frequency above 1 kHz. On comparing with AMO_4 compounds the dielectric constant of the composition seems to be higher. All the compositions show low loss factor values. The values of dielectric constant and very low loss factor indicate the suitability of the sample as a candidate for electronic and dielectric applications.

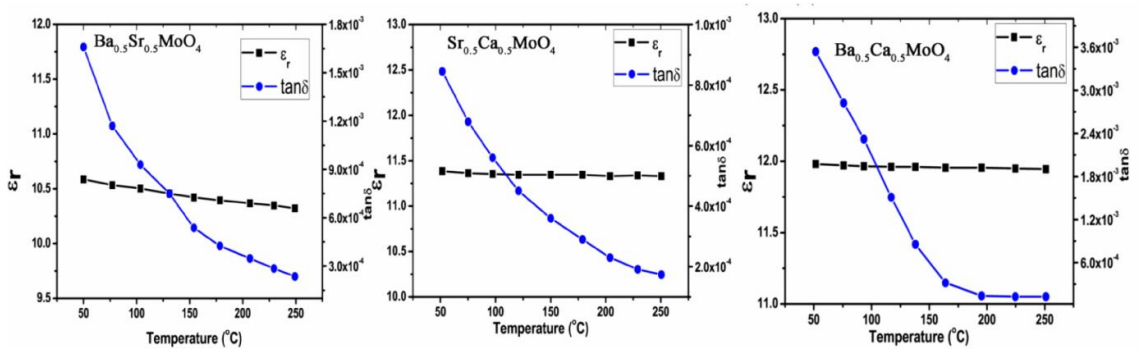

Fig. 9: Variation of ε_r and tanδ with temperature of sintered $A_{0.5}B_{0.5}MoO_4$ (A=B=Ba, Sr, Ca) pellets

The variation of ε_r and tanδ with temperature, in the range 30–250 °C is shown in Figure 9. It is evident from the graph that the variation of dielectric constant with temperature is very minimal in the measured temperature range. The loss factor value lowers with the increase of temperature and is of order 10^{-3} at temperature above 100 °C. The temperature coefficient of dielectric constant (TCK) is determined using the equation given below between temperature 250°C and 30°C at 5MHz.

$$T_{CK} = \left(\frac{\left[\frac{K_{250} - K_{30}}{220} \right]}{K_{30}} \right) \times 10^6 \, \text{ppm}/\circ\text{C}$$

where K_{30} and K_{250} are the dielectric constants at 30 °C and 250 °C respectively, and 220 is the temperature difference.

The obtained T_{CK} values are negative. This indicates that $A_{0.5}B_{0.5}MO_4$ nano powder have relatively low temperature coefficient of dielectric constant when compared to $AMoO_4$. It is clear from the graph that the temperature dependence of dielectric constant is very minimal in the measured range. The loss factor decreases with increase of temperature and is of order 10^{-4} at temperature above 150 °C. Thus nano $A_{0.5}B_{0.5}MO_4$ compositional compounds are suitable for temperature dependent dielectric applications.

The lower dielectric constant and the low loss factor value make nano structured $A_{0.5}B_{0.5}MO_4$ prepared by the present method a promising candidate for LTCC applications, substrate application and as electronic packing materials. That the dielectric constant remains almost constant on heat treatment ensures the suitability of $A_{0.5}Mo_{0.5}MO_4$ and $A_{0.5}W_{0.5}MO_4$ as LTCC material in multi layer circuits.

The main advantage noticed in varying the A^{2+} cation composition in AMO_4 compounds are changes in the dielectric properties. Thus we can infer that the dielectric properties can be fine tuned by adjusting the cation composition, as needed. Thus dielectric constant of these compositional materials can be varied from low to moderate dielectric constant materials with low dielectric loss according to our requirement.

It is also to be noted that even though the sintering temperature of these solid solutions is higher than scheelite compounds, it is less than 950 °C which makes these materials ideal for LTCC applications. As dielectric constant of the solid solution can be lowered or raised, and are low loss materials with negative TCK value, we can finely mould these materials according to our needs. Bivalent metal molybdates and tungstates with scheelite structure allows us to conclude that the chosen solid solutions are excellent luminescent wide band gap materials with moderate dielectric constant and are suitable for numerous optical and electrical properties as discussed.

4. CONCLUSIONS

Nanocrystalline semiconducting $A_{0.5}B_{0.5}MO_4$ (A=B=Ba, Sr, Ca and M=Mo) were synthesized through a modified combustion process. The X-ray diffraction studies have shown that the nanopowder were single phase and possess tetragonal structure. The splitting up of non-degenerate peaks, superposition of certain peaks into a broad peaks, small shift in the vibration mode frequencies, inactivity of certain active peaks in the Raman spectra of the compounds points to lowering of symmetry of the crystal structure. Thus all these compositions possess certain degree of short range structural disorder. FT-IR and Raman spectral analysis confirms the XRD results that the as prepared powder itself is phase pure. TEM analysis confirms the nanocrystalline nature of the sample having particle size in the range of 20–25nm and all the compositions possess nearly spherical morphology. The band gaps of the compositions are found to be higher than $AMoO_4$. The nanocyrstalline $A_{0.5}B_{0.5}MO_4$ are found to be a excellent photo luminescent material with strong green and shows a blue shift in emission wavelength with respect to change of substitutions elements. Thus we can fine tune the emission wavelength from blue to green region according to our needs. These nanocrystals could be sintered at a relatively low temperature in the range 800-875 °C for 3h to a high density. Sintering temperature seems to be increased with respect to AMO4 compound prepared through the same method. The temperature coefficients of dielectric constant for all the samples were negative which makes them suitable for temperature sensitive applications. Thus by varying cationic ration in AMO_4 scheelite system, we can fine tune its properties to the desired values in a limited range. The

low sintering temperature, dielectric constant and minimum loss makes nano $A_{0.5}B_{0.5}MO_4$ excellent composition for low temperature co-fired ceramics, substrate material, and electronic packing materials.

REFERENCES

[1] Feng L. D, Chen X. B, Mao C. J., Mater. Lett., 64, **2010**, 2420 –242
[2] Cui C. H, Bi J., Gao D.J., J. Cryst. Growth, 310, **2008**, 4385–4389.
[3] Yu S.H., Liu B., Mo M.S., Huang J.H., Liu X.M., Qian Y.T., Adv. Funct. Mater., 13, **2003**, 639–647.
[4] Santos M.A., Picon F.C., Escote M.T., Leite E.R., Appl. Phys. Lett., 88, **2006**, 211913–211916.
[5] Sun L., Guo Q., Wu X., Luo S., Pan W., Huang K., Lu J., Ren L., Cao M., Hu C., J. Phys. Chem. C, 111, **2007**, 532–537.
[6] Porto S.L., Longo E., Pizani P.S., Boschi T.M., Simoes L.G.P., Lima S.J.G., Ferreira J.M, Soledade L.E.B, Espinoza J.W.M, Cassia–Santos M.R, Maurera M.A., Paskocimas C.A, Santos I.M.G, Souza A.G, J. Solid State Chem., 181, **2008**, 1876–1881.
[7] Wei L, Liu Y, Lu Y, and Wu T, J. Nanomaterials, 6, **2012**, 1–6.
[8] Zhuravlev V.D., Reznitskikh O.G., Velikodnyi Y. A., Patrusheva T.A., Sivtsova O.V., J Solid State Chemi., 84, **2011**, 2785–2789.
[9] Cho W.S., Yoshimura M., J. Appl. Phys., 83, **1998**, 518–523.
[10] Shi W., Chen J., and Gao S., J. Chinese Ceram. Soc., 39, **2011**, 219–222.
[11] Mohammad Reza Vaezi, Sensor Mater. 20, **2008**, 211–219.
[12] Rao G. N., Chen J. W., Neeleshwar S., Chen Y. Y. and Wu M. K., J. Phys. D: Appl. Phys., 42, **2009**, 095003.
[13] Tomaszewicz E., Kaczmarek S.M., Fuks H., Mater. Chem. Phy., 122, **2010**, 595–601.
[14] Rangappa D, Fujiwara T, Watanabe T, Yoshimura M, Mater. Chem. and Phys., 109, **2008**, 217–223.
[15] Sczancoski J.C., Cavalcante L.S., Joya M.R., Varela J.A., Pizani P.S. and Longo E, Chem. Eng. J., 140(1–3), **2008**, 632–637.
[16] Sczancoski J.C., Cavalcante L.S., Marana N.L., da Silva R.O., Tranquilin R.L., Joya M.R., Pizani P.S., Varela J.A., Sambrano J.R., Siu Li M., Longo E. and Andrese J., Curr. Appl. Phys., 10(2), **2010**, 614–624.
[17] Cavalcante L.S., Sczancoski J.C., Tranquilin R.L., J. Phys. Chem. Solids., 69, **2008**, 2674–2680.
[18] Basiev T. T, Sobol A. A, Voronko Y. K. and. Zverev P. G., Opt. Mater., 15, **2000**, 205–216.
[19] Lim C.S., Mater. Res. Bull., 48, **2013**, 3805–3810.
[20] Thomas J. K., Vidya S., Sam Solomon and Joy K., Materials Science and Engineering, 23, **2011**.
[21] Vidya S., Sam Solomon and Thomas J.K., Phys. Status Solidi A, 209, **2012**, 1067–1074
[22] Vidya S., Sam Solomon and Thomas J.K., Adv. Condensed Matter Phys., **2013**, 2013, 409620.
[23] Vidya S., Sam Solomon and Thomas J.K, Phys. Status. Solidi A, 209, **2012**, 1067–1074.
[24] Campos A. B., Simões A. Z, Longo E, Varela J. A, Longo V. M, de Figueiredo A. T, De Vicente F.S, Hernandes A.C., Appl. Phys. Lett., 91, **2007**, 051923–052100
[25] Marques A.P.A., Motta F.V., Leite E.R, Pizani P.S, Varela J.A, Longo E, de Melo D.M.A., J. Appl. Phys., 104, **2008**, 043505.
[26] Lei H., Zhu X., Sun Y. and Song W., J. Cryst. Growth, 310(4), **2008**, 789–793.
[27] Wang Q., Huo J., Zheng Y., Pang S., He Z., Optic Mater., 35, **2013**, 1146–1150.